Author/s:
Zou, C;Manzie, C;Nešić, D;Kallapur, AG

Title:
Multi-time-scale observer design for state-of-charge and state-of-health of a lithium-ion battery

Date:
2016-12-15

Citation:
Zou, C., Manzie, C., Nešić, D. & Kallapur, A. G. (2016). Multi-time-scale observer design for state-of-charge and state-of-health of a lithium-ion battery. Journal of Power Sources, 335, pp.121-130. https://doi.org/10.1016/j.jpowsour.2016.10.040.

Persistent Link:
https://hdl.handle.net/11343/297959

Multi-Time-Scale Observer Design for State-of-Charge and State-of-health of a Lithium-Ion Battery

Changfu[a,*], Chris Manzie[a], Dragan Nešić[b], Abhijit G Kallapur[a]

[a]*Department of Mechanical Engineering, University of Melbourne, VIC 3010, Australia*
[b]*Department of Electrical and Electronic Engineering, University of Melbourne, VIC 3010, Australia*

Abstract

The accurate online state estimation for some types of nonlinear singularly perturbed systems is challenging due to extensive computational requirements, ill-conditioned gains and/or convergence issues. This paper proposes a multi-time-scale estimation algorithm for a class of nonlinear systems with coupled fast and slow dynamics. Based on a boundary-layer model and a reduced model, a multi-time-scale estimator is proposed in which the design parameter sets can be tuned in different time-scales. Stability property of the estimation errors is analytically characterized by adopting a deterministic version of extended Kalman filter (EKF). This proposed algorithm is applied to estimator design for the state-of-charge (SOC) and state-of-health (SOH) in a lithium-ion battery using the developed reduced order battery models. Simulation results on a high fidelity lithium-ion battery model demonstrate that the observer is effective in estimating SOC and SOH despite a range of common errors due to model order reductions, linearisation, initialisation and noisy measurement.

Keywords: Multi-time-scale observer design, state-of-charge, state-of-health, lithium-ion battery state estimation, electrochemical model, model reduction

1. Introduction

There is an ever-growing trend towards electrifying the powertrain in automotive industry to address the increasingly stringent standards on tailpipe emission and fuel economy. However electric vehicles typically suffer from high relative costs, range anxiety and long charging time [1], which are all related to the battery system. Although lithium-ion batteries have been recognized as a suitable cell chemistry technology for vehicle applications, the properties such as energy/power density, ability to sustain fast "refueling", longevity, and safety are still clearly inferior to their counterpart, the internal combustion engines [2]. Accordingly, advanced management enabling safe and optimal utilization of the battery becomes sought.

For battery management, accurate knowledge of the state-of-charge (SOC) and state-of-health (SOH) is crucial. SOC represents the available capacity remaining in the battery and is often used in the prediction of vehicle's driving range and terminal conditions for battery operations. SOH quantifies the degree of battery degradation and is useful for prediction of life time. SOC and SOH are separately functions of unmeasurable battery internal states, particularly the ion concentrations and capacity fade [3]. This motivates the development of state estimation algorithms for battery systems that monitor the internal states in real-time. However, this is a very challenging task for at least two reasons. First, the underlying dynamics of a lithium-ion battery describing distributed concentration diffusion and local current and potential changes are governed by coupled nonlinear partial differential equations (PDE) [4, 5]. This system model is very computationally expensive so that its use for online estimator design can be impractical. Second, battery dynamics including electrochemical, thermal, electrical, and aging phenomena, exhibit multiple time-scales [6]. Conventional observer design techniques for this singularly perturbed system may lead to ill-conditioned observer gains and potentially undermine the convergence properties [7].

To alleviate potential issues due to model complexity, various estimation algorithms have been proposed based on reduced-order models. Equivalent circuit models (ECMs) are extensively used for battery state estimation because of their relatively simple mathematical structure. For instance, by designing Kalman filter (KF) or its variations, ECMs have been used for battery parameters and/or SOC estimation, e.g. [8, 9, 10] While, ECM-based sliding mode observer (SMO) and particle filter (PF) were proposed for estimation of battery states [11, 12]. Recently, attempts at the estimation of SOC and SOH have been made by using similar models, where the SOH was represented by some parameters [13]. However, in ECMs, battery internal dynamics including concentration diffusion and electrochemical kinetics are essentially ignored. This leads to limited accuracy of these models particularly at an extended operating range. Furthermore, without insights into the system physical limitations [4, 14], the resulting model-based algorithms may be necessarily conservative.

In light of this, reductions for the physics-based battery model are attracting considerable attention. A semi-rigorous approach for systematic simplification of the full PDE models

*Corresponding author
Email address: cezou@student.unimelb.edu.au (Changfu)

has been previously proposed in [5]. The simplified PDE models have been shown a high-fidelity and can be used as a starting point for control-oriented modelling. Using numerical order reduction approaches, partial simplifications have been widely conducted on the temperature model and the electrochemical model, e.g. in [15, 16].

Based on the reduced electrochemistry-based models, a number of papers emerged recently for SOC estimation. Specifically, the single particle model (SPM), where each electrode is assumed to be one lumped particle with only two states representing the system dynamics, were used for state estimation and showed efficient under some operating conditions [17, 18]. However, few papers have been observed in literature to estimate both SOC and SOH using physics-based models. A simplified SPM that neglects the cathode dynamics for SOC and SOH estimation was considered in [19]. This is useful only for the specific batteries where the dynamics in the cathode are much faster than that in the anode and at low and moderate charging rates. Additionally, the aging dynamics have not been explicitly considered. Whilst previous attempts at using physics-based models have been proposed, e.g. [3], they do not directly address the multiple time scales in the problem.

Multi-time-scale estimation theory was studied for a class of linear systems in [20], and was later extended for some nonlinear systems by [7]. In those papers, observer design was realised through restriction of the process dynamics on the slow manifold and thus taking analytical and computational advantages that the lower-dimensional systems bring [21]. Whereas, for the battery case, both the fast and slow states are required for SOC and SOH estimation. Another difficulty is that the battery operates over multiple charge and discharge cycles leading to oscillating states in the electrochemical dynamics.

To address the existing issues in battery state estimation, this article proposes a new algorithm for multi-time-scale observer design. The singularly perturbed systems are decomposed into a boundary-layer (fast) model and a reduced (slow) model using a singular perturbation approach and the averaging theory. Based on these simplified models, a nonlinear observer with fast and slow gains is designed for state estimation of the fast and slow dynamics. This theoretical result is applied to a battery system for estimation of the SOC and SOH. Starting from an initial PDE-based high-fidelity battery model, order reduction techniques are systematically used by gradually introducing relevant assumptions. The obtained models are justified to satisfy the requirements of the proposed multi-time-scale estimation algorithm. The performance of the designed estimator for SOC and SOH is demonstrated via simulations.

The rest of this paper is organized as follows. In Section 2, the theory development for multi-time-scale observer design is presented including clearly stated assumptions and rigorous analysis for stability of the error dynamic systems. This theoretical result is applied to a lithium-ion battery for the estimation of SOC and SOH in Section 3. Simulation results to evaluate the proposed algorithm are provided in Section 4, followed by conclusion of this work in Section 5.

2. Multi-Time-Scale Observer Theory Development

This section describes the development of multi-time-scale estimation algorithm. We consider nonlinear singularly perturbed systems with fast and slow states, $\mathbf{x}_f \in \mathbb{X}_f \subset \mathbb{R}^{n_f}$ and $\mathbf{x}_s \in \mathbb{X}_s \subset \mathbb{R}^{n_s}$, where $\mathbb{X}_f$ and $\mathbb{X}_s$ are bounded sets. u is the system input and $u \in \mathbb{U}$. Particularly in this system, $\mathbf{y}_f$ and $\mathbf{y}_s$ represent the fast and slow measurable system outputs, while, $\mathbf{z}_f$ and $\mathbf{z}_s$ are the unmeasurable system outputs separately in the fast and slow time-scales and belong to the sets of $\mathbb{R}^{m_f}$ and $\mathbb{R}^{m_s}$. ϵ is a perturbation parameter and is small and positive. The system governing equations can be formulated as

$$\dot{\mathbf{x}}_f = F_f\left(\mathbf{x}_f, \mathbf{x}_s, u, \epsilon\right) \tag{1a}$$

$$\dot{\mathbf{x}}_s = \epsilon \mathcal{F}_s\left(\mathbf{x}_f, \mathbf{x}_s, u, \epsilon\right) \tag{1b}$$

$$\mathbf{y}_f = H_f\left(\mathbf{x}_f, \mathbf{x}_s, u, \epsilon\right) \tag{1c}$$

$$\mathbf{z}_f = W_f\left(\mathbf{x}_f, \mathbf{x}_s, \epsilon\right) \tag{1d}$$

$$\mathbf{y}_s = \mathcal{H}_s\left(\mathbf{x}_f, \mathbf{x}_s, \epsilon\right) \tag{1e}$$

$$\mathbf{z}_s = \mathcal{W}_s\left(\mathbf{x}_f, \mathbf{x}_s, \epsilon\right) \tag{1f}$$

Assumption 1. $\epsilon \ll 1$.

If *Assumption 1* holds, from [25] the slow state can be replaced with an equilibrium state $\bar{\mathbf{x}}_s$ and a boundary layer system approximates the fast dynamics, i.e.:

$$\dot{\mathbf{x}}_f(t) = F_f\left(\mathbf{x}_f(t), \bar{\mathbf{x}}_s, u(t), 0\right) \tag{2a}$$

$$\mathbf{y}_f(t) = H_f\left(\mathbf{x}_f(t), \bar{\mathbf{x}}_s, u(t), 0\right) \tag{2b}$$

$$\mathbf{z}_f(t) = W_f\left(\mathbf{x}_f(t), \bar{\mathbf{x}}_s\right) \tag{2c}$$

In the following, an assumption on the stability property of the system (2) is imposed. In the statement, a class-$\mathcal{K}$ function means that a function, $\gamma(\cdot)$, from $\mathbb{R}_{\geq 0}$ to $\mathbb{R}_{\geq 0}$ is continuous, strictly increasing and $\gamma(0) = 0$. A function, $\beta(\cdot, \cdot)$, defined on $\mathbb{R}_{\geq 0} \times \mathbb{R}_{\geq 0}$ taking values in $\mathbb{R}_{\geq 0}$ is said to be a class-$\mathcal{KL}$ function if it is continuous, class-$\mathcal{K}$ function in its first argument, and decreasing to zero in its second argument.

Assumption 2. *$\mathbf{x}_f^*, \mathbf{x}_f^{r*}$ are the solutions of* (1) *and* (2) *for a given u, respectively. There exists an integral manifold $\mathbf{e}_f := \mathbf{x}_f^* - \mathbf{x}_f^{r*}$, a class-$\mathcal{K}$ function γ, and a class-$\mathcal{KL}$ function β such that, for all initial conditions in the domain $\mathbb{X}$, there exists*

$$\left|\mathbf{e}_f(t)\right| \leq \beta(\mathbf{e}_f(0), t) + \gamma(\epsilon) \quad \forall t \geq 0.$$

Given u in this system (2) is time-varying and oscillating, the effect of the fast dynamics on the slow states may be determined predominately by the average of the steady-state behavior of the fast system (2). In particular, this applies when there exists a well-defined average according to the next definition that is a special case of Definition 1 from [22].

Definition 1. *The continuous bounded function $\mathcal{F}_s(\mathbf{x}_f, \mathbf{x}_s, u, \epsilon)$ with its arguments $\mathbf{x}_f, \mathbf{x}_s$ in bounded sets $\mathbb{X}_s, \mathbb{X}_f$, and piecewise differentiable input $u(t) \in \mathbb{U}$, is said to have a well-defined average, F_s, if $\forall \rho > 0$, $\exists T^* > 0$ and $\exists \epsilon^* > 0$ such that $\forall T \geq T^*, \forall \epsilon \in (0, \epsilon^*]$ there exists a measurable function $e : \mathbb{R}_{\geq 0} \to \mathbb{R}^m$ satisfying*

$$\|e(t)\|_\infty \leq \|u(t)\|_\infty \tag{3}$$

such that the following inequality holds

$$\left| \frac{1}{T} \int_0^T \left[\mathcal{F}_s \left(\mathbf{x}_f(t), \mathbf{x}_s, u(t), \epsilon \right) - F_s \left(\mathbf{x}_s, e(t) \right) \right] dt \right| \leq \rho \epsilon \tag{4}$$

The role of $e(t)$ is in *Definition 1* allows an ensemble of solutions for the slow dynamics, if there exist, corresponding to multiple steady-state solutions of the boundary layer system [22].

Assumption 3. *For each $(u, \mathbf{x}_{f0}, \mathbf{x}_{s0}) \in \mathbb{U} \times \mathbb{X}_f \times \mathbb{X}_s$, the functions, $\mathcal{F}_s(\mathbf{x}_f, \mathbf{x}_s, u, \epsilon)$, $\mathcal{W}_s(\mathbf{x}_f, \mathbf{x}_s, \epsilon)$, and $\mathcal{W}_s(\mathbf{x}_f, \mathbf{x}_s, \epsilon)$ from* (1) *have a well-defined average.*

When *Assumptions 1* and *3* are valid, the general average of $\mathcal{F}_s(\mathbf{x}_f, \mathbf{x}_s, u, \epsilon)$ is formulated in the following

$$F_s(\mathbf{x}_s, e) := \frac{1}{T} \int_0^T \mathcal{F}_s \left(\mathbf{x}_f^*(t), \mathbf{x}_s, u(t), 0 \right) dt \tag{5}$$

where $e(t)$ is some measure of $u(t)$ satisfying (3), and $\mathbf{x}_f^* = \mathbf{x}_f^*(\mathbf{x}_{f0}, u(t))$ is the solution of (2) by a specified input $u(t)$ defined over the interval $[0, T]$. Similarly, $\mathcal{W}_s(\cdot), \mathcal{H}_s(\cdot)$ in the output equations can be averaged by setting ϵ in (4) to be zero. The obtained average, $W_s(\cdot), H_s(\cdot)$, are formulated by for a given $u(t)$

$$W_s(\mathbf{x}_s) := \frac{1}{T} \int_0^T \mathcal{W}_s(\mathbf{x}_f(t), \mathbf{x}_s, 0) dt \tag{6}$$

$$H_s(\mathbf{x}_s) := \frac{1}{T} \int_0^T \mathcal{H}_s(\mathbf{x}_f(t), \mathbf{x}_s, 0) dt \tag{7}$$

Based on the average defined above, the reduced (average) system can be obtained, approximating the slow dynamics of the initial system (1b) in the time scale $\tau = \epsilon t$ as

$$\frac{d\mathbf{x}_s}{d\tau} = F_s \left(\mathbf{x}_s, e \right) \tag{8a}$$

$$\mathbf{z}_s = W_s \left(\mathbf{x}_s \right) \tag{8b}$$

Assumption 4. *The system* (8) *has a unique solution $\mathbf{x}_s^*(\tau) \in \mathbb{S}$, for $\tau \in [\tau_0, \tau_1]$, where $\mathbb{S}$ is a compact subset of $\mathbb{X}_s$.*

Remark 1. *Assumptions 2 and 4 are standard in the singular perturbation literature as the model simplification due to time-scale separation can only be justified if the boundary layer dynamics are uniformly asymptotically stable and the solution of the reduced system uniquely exists. These two assumptions hold in many practical systems, including ODE representations of lithium-ion batteries as will be discussed in Section 3.*

To estimate $\mathbf{z}_f(t)$ and $\mathbf{z}_s(\tau)$, the multi-time-scale estimator structure is proposed in the following. For statement, $\hat{\mathbf{x}}_f(t)$ and $\hat{\mathbf{x}}_s(\tau)$ denote the estimates of $\mathbf{x}_f(t)$ and $\mathbf{x}_s(\tau)$, and $K_f(t), K_s(\tau)$ are the estimator gains. By using the nominal battery models obtained in (2) and (8), the dynamic equations for the proposed estimation algorithm are provided

$$\frac{d\hat{\mathbf{x}}_f}{dt} = F_f \left(\hat{\mathbf{x}}_f, \bar{\mathbf{x}}_s, u \right) + K_f \left(\mathbf{y}_f - \hat{\mathbf{y}}_f \right) \tag{9a}$$

$$\hat{\mathbf{y}}_f = H_f \left(\hat{\mathbf{x}}_f, \bar{\mathbf{x}}_s, u \right) \tag{9b}$$

$$\hat{\mathbf{z}}_f = W_f \left(\hat{\mathbf{x}}_f, \bar{\mathbf{x}}_s \right) \tag{9c}$$

$$\frac{d\hat{\mathbf{x}}_s}{d\tau} = F_s \left(\hat{\mathbf{x}}_s, e \right) + K_s \left(\mathbf{y}_s - \hat{\mathbf{y}}_s \right) \tag{9d}$$

$$\hat{\mathbf{y}}_s = H_s \left(\hat{\mathbf{x}}_s \right) \tag{9e}$$

$$\hat{\mathbf{z}}_s = W_s \left(\hat{\mathbf{x}}_s \right) \tag{9f}$$

Note that the multi-time-scale nature of the problem is maintained through $\bar{\mathbf{x}}_s$ in (9a)-(9c) requiring $\hat{\mathbf{x}}_s$ in (9d)-(9f).

The estimation errors are defined as

$$\tilde{\mathbf{x}}_f(t) := \mathbf{x}_f(t) - \hat{\mathbf{x}}_f(t) \tag{10a}$$

$$\tilde{\mathbf{x}}_s(\tau) := \mathbf{x}_s(\tau) - \hat{\mathbf{x}}_s(\tau) \tag{10b}$$

The estimation error dynamics for the fast and slow state variables can be formulated based on (1)-(10)

$$\begin{aligned} \frac{d\tilde{\mathbf{x}}_f}{dt} &= F_f(\mathbf{x}_f, \mathbf{x}_s, u, \epsilon) - F_f(\hat{\mathbf{x}}_f, \bar{\mathbf{x}}_s, u_f) - K_f(\mathbf{y}_f - \hat{\mathbf{y}}_f) \\ &= F_f(\mathbf{x}_f, \bar{\mathbf{x}}_s, u) - F_f(\hat{\mathbf{x}}_f, \bar{\mathbf{x}}_s, u_f) + \xi_f - K_f(\mathbf{y}_f - \hat{\mathbf{y}}_f) \\ &= \left(A_f - K_f C_f \right) \tilde{\mathbf{x}}_f + \xi_f + \Delta_f(\tilde{\mathbf{x}}_f, \mathbf{x}_f, u) \end{aligned} \tag{11a}$$

$$\begin{aligned} \frac{d\tilde{\mathbf{x}}_s}{d\tau} &= \mathcal{F}_s \left(\mathbf{x}_f, \mathbf{x}_s, u, \epsilon \right) - F_s(\hat{\mathbf{x}}_s) - K_s(\mathbf{y}_s - \hat{\mathbf{y}}_s) \\ &= F_s(\mathbf{x}_s, e) - F_s(\hat{\mathbf{x}}_s, e) + \xi_s - K_s(\mathbf{y}_s - \hat{\mathbf{y}}_s) \\ &= \left(A_s - K_s C_s \right) \tilde{\mathbf{x}}_s + \xi_s + \Delta_s(\tilde{\mathbf{x}}_s, \mathbf{x}_s, u) \end{aligned} \tag{11b}$$

where ξ_f, ξ_s represent the model mismatch between the initial model (1) and its simplified counterparts (2) and (8). Additionally,

$$A_f(t) := \frac{\partial F_f}{\partial \mathbf{x}_f} \left(\hat{\mathbf{x}}_f, \bar{\mathbf{x}}_s, u_f \right) \tag{12a}$$

$$C_f(t) := \frac{\partial H_f}{\partial \mathbf{x}_f} \left(\hat{\mathbf{x}}_f, \bar{\mathbf{x}}_s, u_f \right) \tag{12b}$$

$$A_s(\tau) := \frac{\partial F_s}{\partial \mathbf{x}_s} \left(\hat{\mathbf{x}}_s, e \right), \quad C_s(\tau) := \frac{\partial H_s}{\partial \mathbf{x}_s} \left(\hat{\mathbf{x}}_s, e \right) \tag{12c}$$

$$\begin{aligned} \Delta_f := {} & F_f(\mathbf{x}_f, \bar{\mathbf{x}}_s, u) - F_f(\hat{\mathbf{x}}_f, \bar{\mathbf{x}}_s, u_f) - A_f \tilde{\mathbf{x}}_f \\ & - K_f[H_f(\mathbf{x}_f, u_f) - H_f(\hat{\mathbf{x}}_f, u_f) - C_f \tilde{\mathbf{x}}_f] \end{aligned} \tag{13a}$$

$$\begin{aligned} \Delta_s := {} & F_s(\mathbf{x}_s, e) - F_s(\hat{\mathbf{x}}_s, e) - A_s \tilde{\mathbf{x}}_s \\ & - K_s[H_s(\mathbf{x}_s) - H_s(\hat{\mathbf{x}}_s) - C_s \tilde{\mathbf{x}}_s] \end{aligned} \tag{13b}$$

Assumption 5. *The functions, $F_f, F_s, H_f, H_s, W_f, W_s$, from* (2)-(8) *are Lipschitz continuous in their arguments. Furthermore, $\mathbf{x}_f, \mathbf{x}_s$ and u is bounded.*

Assumption 6. *For the Jacobian matrices, A_f, A_s, C_f, C_s, from* (12)*, the pairs (A_f, C_f) and (A_s, C_s) are both uniformly observable.*

Assumption 7. *There exists an extended Kalman filter (EKF) gain trajectory, $K(t)$, so that in the system* (11)*, $\tilde{\mathbf{x}}_f$ and $\tilde{\mathbf{x}}_s$ are semi-globally practically stable. Namely, there exist positive constants $c_f, c_s, k_f, k_s, \lambda_f, \lambda_s$ and functions $\gamma_f(\cdot), \gamma_s(\cdot) \in \mathcal{K}$ such that $\forall t > t_0 > 0$*

$$\begin{aligned} &\left\|\tilde{\mathbf{x}}_f(0)\right\| \le c_f, \ \ \|\tilde{\mathbf{x}}_s(0)\| \le c_s \\ \Rightarrow &\left\|\tilde{\mathbf{x}}_f(t)\right\| \le k_f e^{-\lambda_f(t-t_0)} + \gamma_f\left(\left\|\xi_f(t)\right\|_{max}\right), \\ &\|\tilde{\mathbf{x}}_s(\tau)\| \le k_s e^{-\lambda_s(\tau-t_0)} + \gamma_s\left(\|\xi_s(\tau)\|_{max}\right) \end{aligned}$$

Remark 2. *Assumption 7 may be potentially relaxed to a more general case which covers other nonlinear estimation algorithms in addition to EKF. In this case, the method of [23], where only the slow states of singularly perturbed systems are of interest and estimated, can be possibly extended for estimator design around the boundary-layer model and slow model separately for the slow and fast states.*

In the following proposition, the main theoretical result of this paper is presented. The errors in estimation of $\mathbf{z}_f$ and $\mathbf{z}_s$ are defined as $\tilde{\mathbf{z}}_f(t) := \mathbf{z}_f(t) - \hat{\mathbf{z}}_f(t)$, and $\tilde{\mathbf{z}}_s(\tau) := \mathbf{z}_s(\tau) - \hat{\mathbf{z}}_s(\tau)$.

Proposition 1. *Let Assumptions 1-7 hold. Consider the observer* (9) *applied to estimate $\mathbf{z}_f$ and $\mathbf{z}_s$ in* (1)*, if there exist positive constants d_f, d_s, $\mathcal{KL}$ functions β_f, β_s, and $\mathcal{K}$ functions γ_f, γ_s such that for all $t \in [t_0, t_1]$, $\tau \in [\tau_0, \tau_1]$, $\left\|\tilde{\mathbf{z}}_f(0)\right\| \le d_f$ and $\|\tilde{\mathbf{z}}_s(0)\| \le d_s$, there exist*

$$\left|\tilde{\mathbf{z}}_f(t)\right| < \beta\left(\left|\mathbf{z}_{f0} - \hat{\mathbf{z}}_{f0}\right|, t\right) + \gamma_f(\epsilon) \tag{14a}$$

$$|\tilde{\mathbf{z}}_s(\tau)| < \beta\left(|\mathbf{z}_{s0} - \hat{\mathbf{z}}_{s0}|, \tau\right) + \gamma_s(\epsilon) \tag{14b}$$

where β is a class-$\mathcal{KL}$ function, $\gamma_f > 0$, $\gamma_s > 0$ and are class-$\mathcal{K}$ functions, $t \in [t_0, t_1]$ and $\tau \in [\tau_0, \tau_1]$.

Sketch of proof. The inequality relationship in (14a) is rewritten in view of *Assumption 5* as

$$\begin{aligned} \left|\tilde{\mathbf{z}}_f(t)\right| &= \left|W_f\left(\mathbf{x}_f(t), \mathbf{x}_s(t)\right) - W_f\left(\hat{\mathbf{x}}_f(t), \bar{\mathbf{x}}_s\right)\right| \\ &\le L_1\left|\mathbf{x}_f(t) - \hat{\mathbf{x}}_f(t)\right| + L_2\left|\mathbf{x}_s(t) - \bar{\mathbf{x}}_s\right| \\ &< \beta\left(\left|\mathbf{z}_{f0} - \hat{\mathbf{z}}_{f0}\right|, t\right) + \gamma_f(\epsilon) \end{aligned} \tag{15}$$

Based on *Assumptions 4-7*, and following the procedure of *Lemma 11.2* in [24], the $|\mathbf{x}_f(t) - \hat{\mathbf{x}}_f(t)|$ in (15) can be readily shown to be semi-globally practically stable and the final error ball is determined by $\left\|\xi_f\right\|_{\max}$. In consideration of 1-2 and Tikhonov's theorem [25], it can be obtained that $|\mathbf{x}_s(t) - \bar{\mathbf{x}}_s| = O(\epsilon)$, $\forall t \in [t_b, t_1]$. Therefore, (14a) has been proved. The similar work can be conducted to prove (14b).

Remark 3. *Proposition 1 implies the mismatch between the initial system* (1) *and the decoupled systems,* (2) *and* (8)*, can be compensated by the designed estimator. That is, the errors in estimation of $\mathbf{z}_f$ and $\mathbf{z}_s$ converge in an asymptotic manner to some bounded sets, although the design process of the multi-time-scale observer is simplified relative to conventional estimation approaches. More importantly, the time scales of the convergence are different for the fast and slow error dynamics.*

3. Application of Multi-Time-Scale Observer To Li-Ion Battery

The system dynamics for a lithium-ion battery include electrochemical, thermal, electrical, and ageing behaviors and are originally governed by a set of coupled nonlinear PDEs. Time-scale separation techniques may be applied to this battery model for system simplification. To do so, justification for the underlying assumptions on the battery system is first conducted.

Justification for *Assumption 1*: This can be readily justified by comparing the time constants corresponding to battery electrochemical-thermal dynamics and ageing dynamics. Using typical lithium-ion batteries and excitation of the current, as discussed in [5], the electrochemical-thermal states show significant variations within minutes. In contrast, the degree of ageing dynamics is several orders of magnitude slower than the normal intercalation reactions. Therefore, in the fast time-scale, the slow dynamics as well as the associated singular perturbation parameter is negligibly small.

Justification for *Assumptions 2-4*: For this initial battery model, the stability property of its boundary layer model and the solution existence of its average model have been shown in [5].

Note that the initial nonlinear PDE battery model and its Hilbert space reformulation were completely described in [6] and are not provided in this work to avoid duplications. Given *Assumptions 1-4* are valid for the battery system, singular perturbation techniques and the averaging theory can be systematically applied to the initial model. As a consequence, a fast model that captures the electrochemical-thermal dynamics and a slow model governing the ageing process can be derived. These two PDE models, referred to as Σ_f and Σ_s, will be employed for further model reductions to estimate battery SOC and SOH.

3.1. Battery model: fast dynamics

The generic multi-time-scale observer design algorithm in the previous section will now be formulated with battery models approximating the PDE models, Σ_f and Σ_s. The first step is to define the fast state vector as $\mathbf{x}_f = [C_s^-(t), q_s^-(t), C_e^-(t)]^T$. The applied current density, $I(t)$, is taken as the system input. To facilitate statement of the battery system, the notations provided in Table 1 are used. These states are sufficient to capture the fast dynamics under the following assumptions

Assumption 8. *The battery temperature can be approximated by a lumped value and it is measurable.*

Remark 4. *While the temperature dynamics have a significant effect on battery SOH, a lumped battery temperature has been assumed and justified previously in a number of papers, e.g. [26].*

Assumption 9. *The spatial and temporal trajectory of ion concentrations, $C = [C_s^{\pm}(x, r, t); C_e^{\pm,sep}(x, t)]$, can be approximated*

Table 1: Nomenclature

a	Interfacial area of solid particles
C_s	Li-ion concentration in solid particles
C_e	Li-ion concentration in the electrolyte
D_s	Effective electric diffusion coefficient
D_e	Effective ionic diffusion coefficient
F	Faraday's constant
i_0	Exchange current density of the normal reaction
i_{0sr}	Exchange current density of the side reaction
J_I	Normal ion flux at the surface of solid particles
J_{sr}	Side reaction ion flux
k	Reaction Rate in the electrode
$L^{\pm}$	Length of the negative/positive electrode
Q_{sr}	Capacity fade
q_s	Volume-averaged concentration flux
R_p	Radius of the solid particles
R_f	SEI film resistance
R	Universal gas constant
η	Overpotential of the normal reaction
γ	Transference number of the anion
κ	Effective ionic conductivity in the electrolyte
σ	Effective electronic conductivity in the electrode
μ_e	Liquid-phase volume fraction
Φ_e	Local potential in the electrolyte

by

$$\hat{C}(x,r,t) = \sum_{i=1}^{n} \vartheta_i \cdot \gamma(r) \cdot \alpha(x) \cdot \phi_i(t) \tag{16}$$

such that there exists:

$$\left|C(x,r,t) - \hat{C}(x,r,t)\right| < \epsilon(n),\ \forall t \geq 0$$

where $\phi(\cdot)$ is a basis function, and $\epsilon(\cdot)$ is an $\mathcal{L}$-function.

Remark 5. *The equation* (16) *can be realised by polynomial approximations. Specifically, according to [27] the solid-phase concentration can be well approximated by the fourth order polynomial*

$$\hat{C}_s(x,r,t) = d_1(x,t) + d_2(x,t)\frac{r^2}{R_P^2} + d_3(x,t)\frac{r^4}{R_P^4}$$

Similarly, at constant applied current, the electrolyte concentration has been shown to be well captured by using $n = 2$ in (16) *[28], i.e.*

$$\hat{C}_e(x,t) = (p_1 x^2/2 + p_2) \cdot f(t) \cdot I(t) + C_{e0}$$

To capture electrolyte characteristics under time-varying currents as well, this approximation may be extended using

$$\hat{C}_e(x,t) = (p_1 x^2/2 + p_2) \cdot f\,(t, I(t)) + C_{e0}$$

Further simplification typically involves removing the x-coordinate dependency from the concentration states by considering one-node discretisation in $\hat{C}_s$ and by defining $x = 0$ in $\hat{C}_e$.

Assumption 10. *The net flow between the solid-phase and liquid-phase Li-ion concentrations over all the domains of a battery cell is negligibly small.*

Remark 6. *This can be justified by comparing the magnitudes of the total ions in the electrolyte, n_{Li}^l, and the total solid-phase ions, n_{Li}^s. Simulations using typical battery parameters, e.g. [29] show that $n_{Li}^l < 4\% \cdot n_{Li}^s$.*

Based on *Assumptions 8-10* and their remarks, the initial infinite dimensional battery model of Σ_f is approximated by an ODE model. The resulting fast battery dynamics representing $F_f(\cdot)$ in (2) are then given by

$$F_f\left(\mathbf{x}_f, u\right) = \begin{bmatrix} -\dfrac{3}{FL^- a^- R_p^-} I(t) \\ -\dfrac{30 D_s^-}{(R_p^-)^2} q_s^-(t) - \dfrac{22.5}{F a^- L^- (R_p^-)^2} I(t) \\ \dfrac{D_e^- p_1^-}{\mu_e^- p_2^-}\left(C_e^-(t) - C_{e0}\right) + \dfrac{\gamma^-}{FL^-\mu_e^-} I(t) \end{bmatrix} \tag{17}$$

The outputs of interest for the fast dynamic model include the terminal voltage and the SOC in the form of

$$\begin{aligned} \mathbf{y}_f :=& V(t) = \Phi_e^+(t) - \Phi_e^-(t) + U^+\left(C_{ss}^+(t)\right) \\ & - U^-\left(C_{ss}^-(t)\right) + \eta^+(t) - \eta^-(t) - \frac{R_f(t_0) I(t)}{a^- L^-} \end{aligned} \tag{18a}$$

$$\mathbf{z}_f := SOC(t) = \frac{C_s^-(t)}{C_{\text{smax}}^-} \tag{18b}$$

where

$$\eta^{\pm}(t) = \pm \frac{2RT_m}{F} \operatorname{asinh}\left(\frac{-I(t)/(2a^{\pm}k^{\pm}L^{\pm})}{\sqrt{C_e^{\pm}(t)(C_{\text{smax}}^{\pm} - C_{ss}^{\pm}(t))C_{ss}^{\pm}(t))}}\right) \tag{19a}$$

$$\begin{aligned} \Phi_e^+(t) - \Phi_e^-(t) =& \frac{2RT_m}{F}\left(\gamma^+ \ln C_e^+(t) - \gamma^- \ln C_e^-(t)\right) \\ & - \left(\frac{L^-}{2\kappa^-} + \frac{L^{sep}}{\kappa^{sep}} + \frac{L^+}{2\kappa^+}\right) I(t) \end{aligned} \tag{19b}$$

$$C_s^+(t) = \frac{L^+\mu_s^+ C_{s0}^+ + L^-\mu_s^- C_{s0}^- - L^-\mu_s^- C_s^-(t)}{L^+\mu_s^+} \tag{19c}$$

$$C_s^+(t_f^+) = C_s^+(t_f^-) - \frac{Q_{sr}(t_f) - Q_{sr}(t_0)}{Q_{\max}} C_s^+(t_f^-) \tag{19d}$$

$$C_e^+(t) = -\frac{L^-\mu_e^-}{L^+\mu_e^+}\left(C_e^-(t) - C_{e0}\right) + C_{e0} \tag{19e}$$

$$q_s^+(t) = -\frac{(R_p^+)^3 L^-\mu_s^-}{(R_p^-)^3 L^+\mu_s^+} q_s^-(t) \tag{19f}$$

$$C_{ss}^+(t) = C_s^+(t) + \frac{8R_p^+}{35} q_s^+(t) + \frac{R_p^+}{35 F a^+ L^+ D_s^+} I(t) \tag{19g}$$

In (18a) and (19d), the slow states R_f and Q_{sr} appear but are regarded as constant. t_0 and t_f are separately the initial and end time of an operating cycle.

To assess the validity of the reduced ODE model, the reduced model and the original PDE model are compared where the input current is taken from an urban dynamometer driving schedules (UDDS) driving test. The parameters to be used in simulations are adopted from [5]. The model fidelity is assessed

through the normalised absolute error in the states and output with the definition of

$$\beta_w(t) = \left| \frac{w_r(t) - w(t)}{w_{\max}} \right| \tag{20}$$

where $w_r(t)$, $w(t)$ are separately solutions of the reduced model and the high-fidelity model, and $w_{\max}$ is the maximum value of $w(t)$. The comparison results are illustrated in Fig. 1.

The profile of solid-phase Li-ion concentration derived from the reduced model closely matches solution of the initial model. Similarly, a good agreement is achieved in the electrolyte concentration. Accurate computations imply the SOC will also be modelled accurately. Although the error in voltage prediction is seen to become larger at higher charging rates or step changes of the input, the reduced model is a good representation of the initial model with the error in the entire operating cycle bounded by 2%. This level of model mismatch is within an acceptable range for typical observer design.

3.2. Battery model: slow dynamics

The slow state vector is defined as $\mathbf{x}_s = [Q_{sr}(t), R_f(t)]^T$. These state dynamics are governed by (1b) with the function, $\mathcal{F}_s(\cdot)$, is formulated as [5]

$$\epsilon \mathcal{F}_s\left(\mathbf{x}_f, \mathbf{x}_s, u, \epsilon\right) = \begin{bmatrix} \epsilon a^- A^- L^- i_0 \exp\left(\dfrac{-F\alpha_{sr}\eta_{sr}(t)}{RT_m}\right) \\ \epsilon \dfrac{M_f i_0}{F\rho_f \sigma_f} \exp\left(\dfrac{-F\alpha_{sr}\eta_{sr}(t)}{RT_m}\right) \end{bmatrix} \tag{21}$$

where σ_f, M_f, ρ_f are respectively the conductivity, average molecular weight, and average density of the SEI film; A is the equivalent cross-sectional area. $\epsilon := i_{0sr}/i_0$. The overpotential, η_{sr}, determines battery side reaction rate and is formulated

$$\eta_{sr}(t) = \Phi_s^-(t) - \Phi_e^-(t) - U_{sr} - FR_f(t)\left[J_I^-(t) + \epsilon \frac{-i_0}{F} \exp\left(\frac{-F\alpha_{sr}\eta_{sr}(t}{RT_m}\right)\right] \tag{22}$$

The system outputs of the slow battery model (8) are given in the form of

$$z_s := SOH(t) = \frac{Q_{\max} - Q_{sr}(t)}{Q_{\max}} \tag{23a}$$

$$y_s := R_f(t) \tag{23b}$$

To permit close-loop estimator design for the SOH during cycling operations, in this work it is considered to measure the resistance, R_f, at the end of each operating cycle via electrochemical impedance spectroscopy (EIS). Details for the EIS technique can be referred to [30].

3.3. Multi-time-scale battery observer

The proposed multi-time-scale algorithm is applied in this section to estimate SOC and SOH of a lithium-ion battery. The parameters for simulations are taken from [5, 29]. Based on the obtained models, which are denoted by Σ_f^r and Σ_s^r, the observer

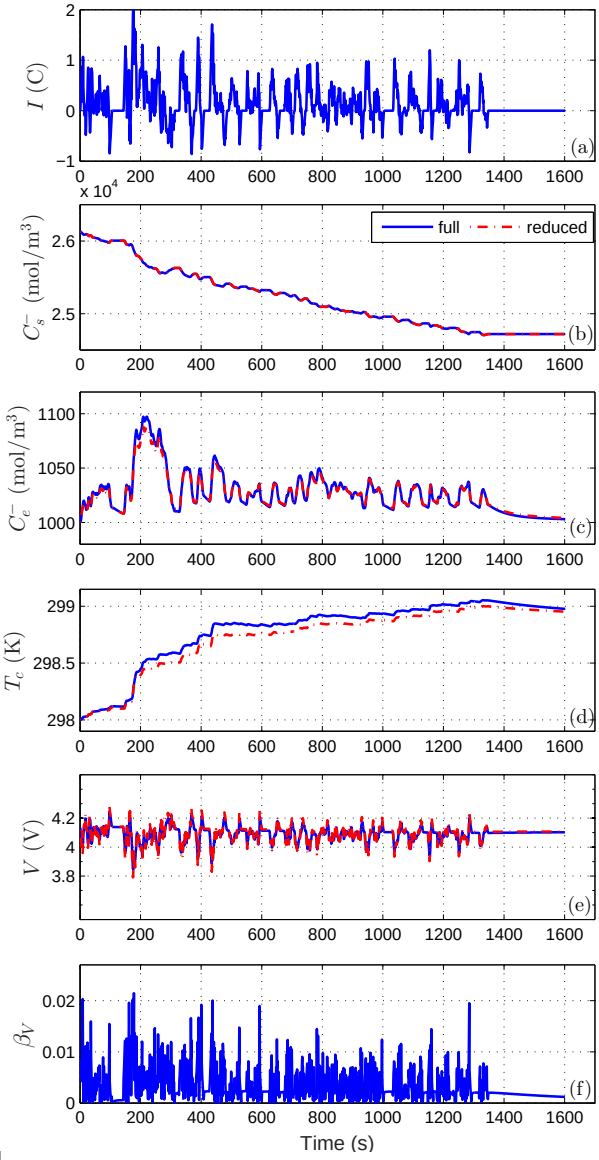

Figure 1: Open-loop comparison of the initial model and the reduced model.

with fast and slow dynamics is designed in this subsection. This algorithm for state estimation is illustrated in Fig. 2.

The system model (8) requires evaluation of the averaged function $F_s(\mathbf{x}_s, e)$, which implicitly assumes same charging strategy is used in each cycle. In this work, the averaged function $F_s(\mathbf{x}_s, e)$ is approximated using a two-step process.

The first step is to generate the mapping $F_s(\mathbf{x}_s, \text{SOC}, u)$, where u, SOC are specified at a series of constant values. The battery is charged to a fixed SOC value and then experiences a discharge operation to the initial SOC. This is followed by a relaxed period to recover the equilibrium state. This whole process is defined as a "cycle" with the period of T. To enable the same capacity is delivered in each cycle, no any voltage constraint is enforced in the course of operations. When the system input is specified at a constant value u at the time interval $[0, T]$ and the slow states are fixed at their equilibrium state, *i.e.* constant values in this case, the fast battery model can be run to

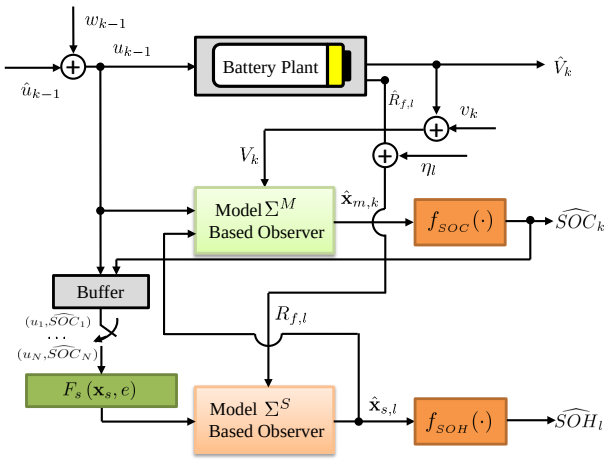

Figure 2: Multi-time-scale observer design algorithm for battery SOC and SOH estimation.

reproduce the solution of the fast states, $\mathbf{x}_f^*(t)$. The trajectory of the fast states can be then substituted into (5) to derive the function, $F_s(\cdot)$, according to

$$F_s(\mathbf{x}_s, \mathrm{SOC}^i, u^i) = \begin{bmatrix} \dfrac{a^- A^- L^- i_0}{T} \displaystyle\int_0^T \exp\left(\frac{-F\alpha_{sr}\eta_{sr}(t)}{RT_m}\right) dt \\ \dfrac{M_f i_0}{F\rho_f \sigma_f T} \displaystyle\int_0^T \exp\left(\frac{-F\alpha_{sr}\eta_{sr}(t)}{RT_m}\right) dt \end{bmatrix} \tag{24}$$

and the overpotential, η_{sr}, from (22) is re-formulated by setting $\epsilon = 0$ and $u(t) = u^i$ as

$$\eta_{sr}(t) = \Phi_s^-(t) - \Phi_e^-(t) - U_{sr} - \frac{R_f(t_0)u^i}{a^- L^-} \tag{25}$$

SOC^i in the function $F_s(\cdot)$ can be understood in some sense as an average measure of the fast states under the current u^i. In other words, there exists a solution: $\mathrm{SOC} = \mathrm{SOC}(\mathbf{x}_{f0}, \bar{\mathbf{x}}_s, u, t)$.

By sequentially performing this process with different u^i over multiple cycles and multiple depths of charge, the map, $F_s(\mathbf{x}_s, \mathrm{SOC}, u)$, can be generated. Fig. 3(a)-(b) illustrate this 3D map by respectively fixing the SOC and $\mathbf{x}_s$. It can be clearly seen that $F_s(\cdot)$ greatly increases at larger values of SOC or u. Whilst the impact of $\mathbf{x}_s$ is negligibly small, indicating that the degradation rate is (almost) independent of the battery's SOH. It is worth noting that this map can be generated offline, and is expected to be used for online state estimation.

Step 2 in the approximation of $F_s(\mathbf{x}_s, e)$ for general $u(t)$ and $\mathrm{SOC}(t)$ is to use a piecewise constant current in (24) and the summation of $F_s(\mathrm{SOC}^i, u^i)$ along the trajectory:

$$\hat{F}_s(\mathbf{x}_s, e) := \frac{1}{N} \sum_{i=1}^{N} F_s(\mathrm{SOC}^i, u^i) \cdot \Delta t \tag{26}$$

where Δt is the sampling time, and u^i is a constant value approximating $u(t)$ over the time period of $[i, i+1]\Delta t$.

Assumption 11. *For any given charging strategy, $u(t)$, and $\mathbf{x}_s \in \mathbb{X}_s$, $\hat{F}_s(\mathbf{x}_s, e)$ in (26) and $F_s(\mathbf{x}_s, e)$ are sufficiently close.*

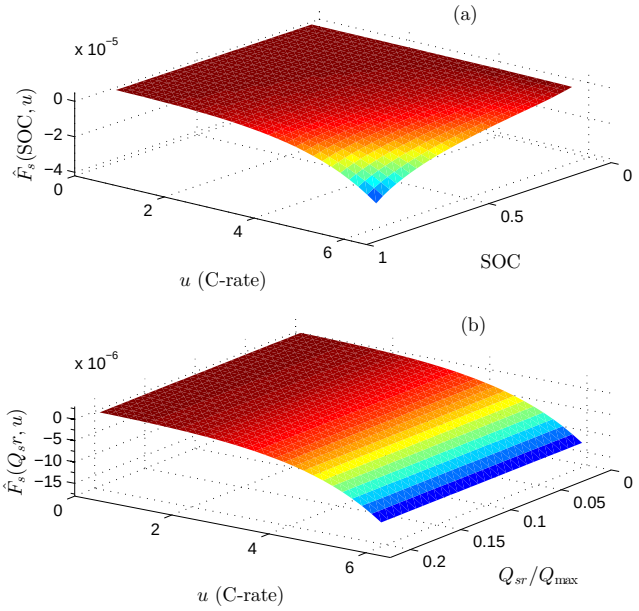

Figure 3: The map of battery degradation rates at different charging C-rates, capacity fade and SOC. (a) the $Q_{sr}/Q_{\max}$ is fixed at 0; (b) the SOC change in each cycle is fixed at 0.45–0.55. Unit of $\hat{F}_s$: 1/sec.

Justification for *Assumption 11*: This is examined in terms of several typically used charging strategies, including the constant-current constant-voltage (CCCV) charging and multi-stage-CC (MCC) charging. For the MCC algorithm, the battery is charged under a large constant-current in the beginning, and is then charged by lower constant-currents for further several stages. For each charging strategy, the battery is started from the same initial states. The simulation results for both the charging strategies are given in Fig. 4. It is found that the profiles of $\hat{F}_s$ closely follow its counterpart F_s, while the errors over 200 cycles in prediction of battery SOH are within 1%. At such a scale of errors, it is reasonable to use the approximation in (26). Furthermore, for battery state estimation, the existing errors are supposed to be compensated by the designed robust estimator.

In addition to the justification of *Assumptions 1-4* shown before, the validity of other assumptions underpinning *Proposition 1* is examined on the developed battery models.

Justification for *Assumption 5*: It can be easily founded that in the reduced models, Σ_f^r and Σ_s^r, the functions, F_f, F_s, H_f, W_f, W_s, are Lipschitz continuous. The requirement on bounded states and input also follows the nature of practical battery charge and discharge operations.

Justification for *Assumption 6*: The local observability can be examined by calculating the corresponding observability matrix $O = [C; CA; \cdots; CA^{n-1}]$ for both the slow and fast models. By means of numerical calculation, the rank of observability matrices for both the battery models during operations can be obtained and are shown in Fig. 5. Given the full rank is obtained over the whole estimation process, the two reduced models are thus fully observable in a linear sense.

Proposition 1 relies on the use of an EKF, as depicted in *As-*

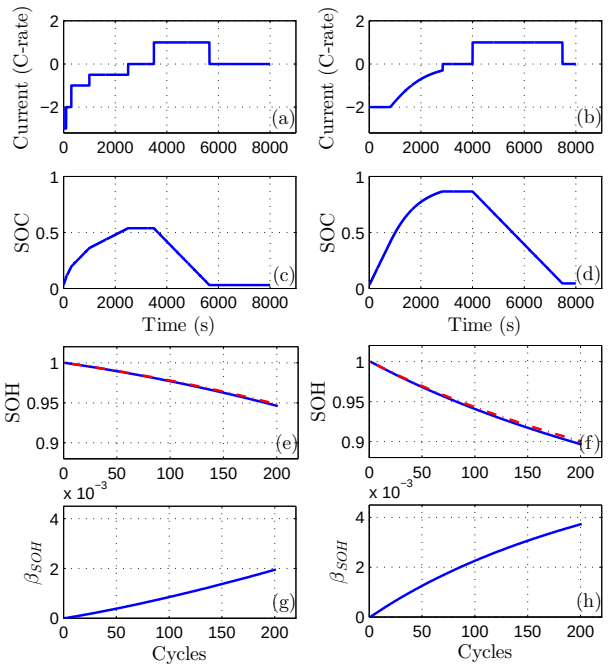

Figure 4: The quasi-steady-state map, $F_s(\mathbf{x}_s, e)$, and its approximation, $\hat{F}_s(\mathbf{x}_s, e)$, for different charging strategies. The left-hand-side shows the MCC charging results, while the right-hand-side presents the CCCV charging results. F_s is drawn in blue solid line, and $\hat{F}_s$ is represented by the red dot-dashed line.

sumption 7. However, as noted in *Remark 2* , it may be possible to replace the EKF with other estimators. Here both the EKF, and an unscented Kalman filter (UKF) alternative are considered, although the latter is not currently shown to satisfy *Proposition 1*.

Justification for *Assumption 7*: The EKF design method can be implemented based around the models Σ_f^r and Σ_s^r. Within the framework of continuous-time EKF, the gains, $K_f(t)$ and $K_s(\tau)$, are calculated from

$$K_f = P_f C_f^T (C_f P_f C_f^T + R_f)^{-1} \tag{27a}$$

$$K_s = P_s C_s^T \left(C_s P_s C_s^T + R_s\right)^{-1} \tag{27b}$$

The covariances in (27), $P_f(t)$ and $P_s(\tau)$, are propagated and updated through (28)

$$\dot{P}_f = A_f P_f + P_f A_f^T + Q_f - P_f C_f^T R_f^{-1} C_f P_f \tag{28a}$$

$$P_f(0) = P_{f0} \tag{28b}$$

$$\dot{P}_s = A_s P_s + P_s A_s^T + Q_s - P_s C_s^T R_s^{-1} C_s P_s \tag{28c}$$

$$P_s(0) = P_{s0} \tag{28d}$$

where, A_f, A_s, C_f, C_s are the Jacobian matrices defined in (12), Q represents covariances of the process noises, and R denotes covariances of the measurement noise.

Unlike the stochastic sampling technique used in the EKF, the unscented transform is used to pick a minimal set of sigma points around the mean. These sigma points are directly propagated through the nonlinear models of Σ_f^r and Σ_s^r. The mean and covariance of the estimate are then recovered from the sigma points. The mathematical equations for UKF propagation and update are not repeated here but the readers are referred to literature such as [31].

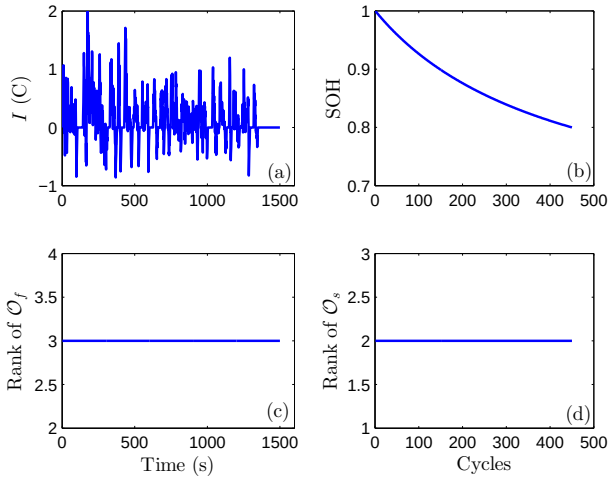

Figure 5: Observability of the developed battery models, Σ_f^r and Σ_s^r.

When all the assumptions are satisfied, we are allowed to design an appropriate observer for SOC and SOH estimation using the derived battery models and the methodology of multi-time-scale observer design. With the state $\hat{\mathbf{x}}_f$ and $\hat{\mathbf{x}}_s$ obtained from the observers, $\hat{z}_{\text{SOC}}$ and $\hat{z}_{\text{SOH}}$ can be calculated according to their output functions. In this proposed estimation algorithm, the design parameters, including (P_{f0}, Q_f, R_f) and (P_{s0}, Q_s, R_s), can be tuned separately in different time-scales without risk of ill-conditional gains and restriction of the convergence properties.

4. Simulation Results

To demonstrate the proposed multi-time-scale estimation methodology, simulations are conducted on a lithium-ion battery. The estimated states are validated against the results from the original high-fidelity battery model described in [5].

4.1. Estimation results in fast time-scale (SOC)

To test the proposed estimation algorithm in terms of the fast dynamics, the UDDS current shown in Fig. 1 is employed as the system input. To check the robustness of the proposed estimator, additional white Gaussian noise with a standard deviation of 5mV is added to the voltage measurement. In addition, the fast time-scale states are initialised with 50% initial errors.

Fig. 6 depicts the estimation results regarding the terminal voltage and SOC by using EKF and UKF. It can be seen that the estimated states using both the EKF and UKF converge to the true values rapidly from the imposed initial error. Furthermore, the steady-state errors are less than 1% for the terminal voltage and less than 3% for the SOC.

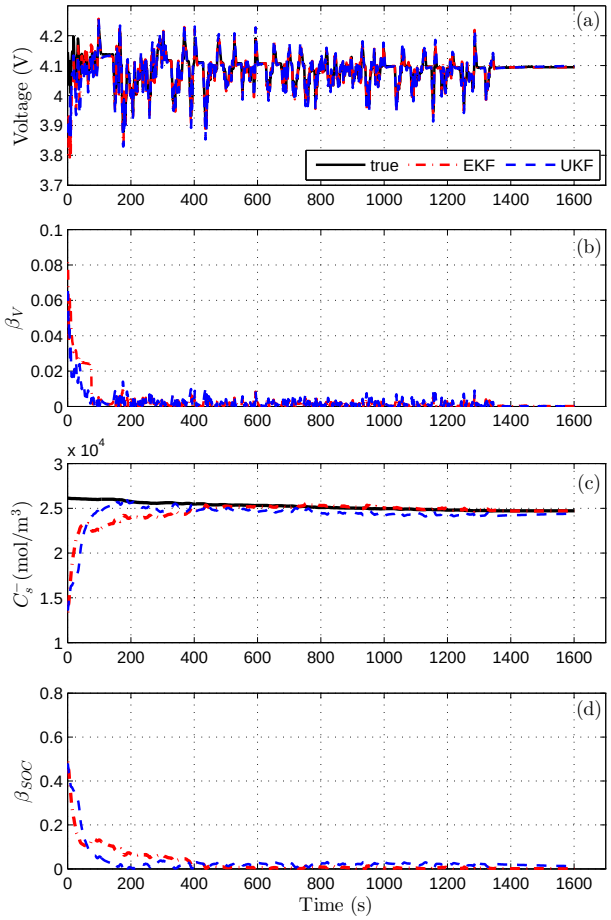

Figure 6: Estimation results of the terminal voltage and SOC under validated against the true values. (a) The terminal voltage. (b) The relative absolute error in voltage estimation. (c) The ion concentration in the anode particle. (d) The relative absolute error in SOC estimation.

In this case, the UKF has similar accuracy to the EKF. While the UKF exhibits slightly faster convergence in this simulation, it comes at increased computational expense.

4.2. Estimation results in two time-scales (SOC + SOH)

A multi-stage CC charging protocol is now considered to investigate the multi-time-scale estimation of SOC and SOH. The battery is charged with multi-stage constant-current, where the current is 2.5C, 1.5C, 1C, and 0.5C, respectively, as shown for one cycle in Fig. 7. Each time the terminal voltage reaches the maximum safe voltage level of 4.2V, the current is switched to a lower current. A relaxed period is maintained when the battery is fully charged. The discharging operation occurs at 1C until the terminal voltage drops to 3.3V, followed by a final relax period. In this simulation, all the slow states are initialised with 10% initial errors, while the fast time-scale states are initialised with 20% errors.

Simulations for the designed estimator over 450 cycles are conducted under the specified charging protocol. Fig. 8 illustrates the estimation result for SOC and SOH, where the SOC trajectory of its first 40 cycles is provided for well visualisation.

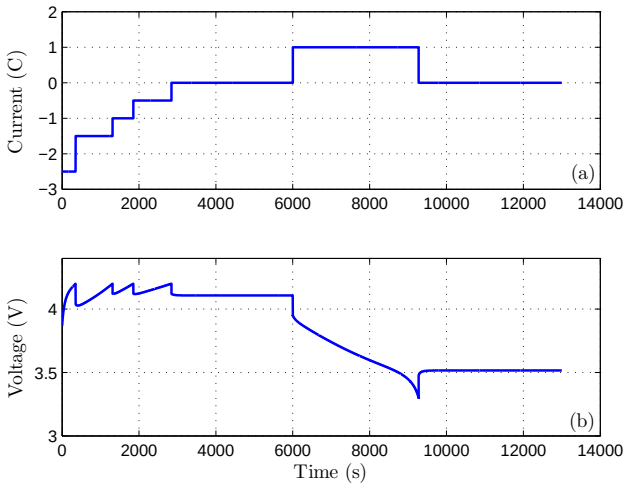

Figure 7: The current and voltage profiles in the 4-stage CC charging protocol.

By deliberately using relatively high charging rates, one observation from this figure is that the battery degrades to its end of life, *i.e.*, 80% of the initial SOH, in these operating cycles. Regarding the estimation performance, the designed EKF is found to quickly reject the initial error at the fast states within the first 0.1 cycles, and the slow state initial errors are rejected within 10 cycles.

All the estimated states converge to the vicinity of their true values. The steady-state estimation errors in the SOC and SOH are bounded by 3%. These results verify *Assumption 7* and demonstrate the effectiveness of the proposed multi-time-scale estimation algorithm.

For comparison, the proposed multi-time-scale estimator is also implemented with a UKF. It shows similar results as the EKF in the estimation accuracy but faster convergence can be potentially obtained, albeit again at increased computation cost. This indicates there is merit in extending *Assumption 7* to consider wider classes of estimation algorithms.

Based on this analysis, the designed nonlinear robust estimator for SOC and SOH within the multi-time-scale estimation framework is effective in dealing with model mismatch, initial errors and noise. While, steady-state errors have been observed in the estimation results, this is consistent with theoretical analysis in Section 2. That is, exact convergence to the origin for the estimation errors is not possible due to the presence of uncertainties.

In this work, the accuracy of simplified models has been validated against the initial battery model. Although a dominant aging mechanism namely SEI film based aging has been considered in this model, various factors may contribute to battery SOH change. The identification and quantification of all aging mechanisms are still an ongoing work. It is important for readers to note that a different SOH model can be easily fitted into the proposed methodology of multi-time-scale estimation.

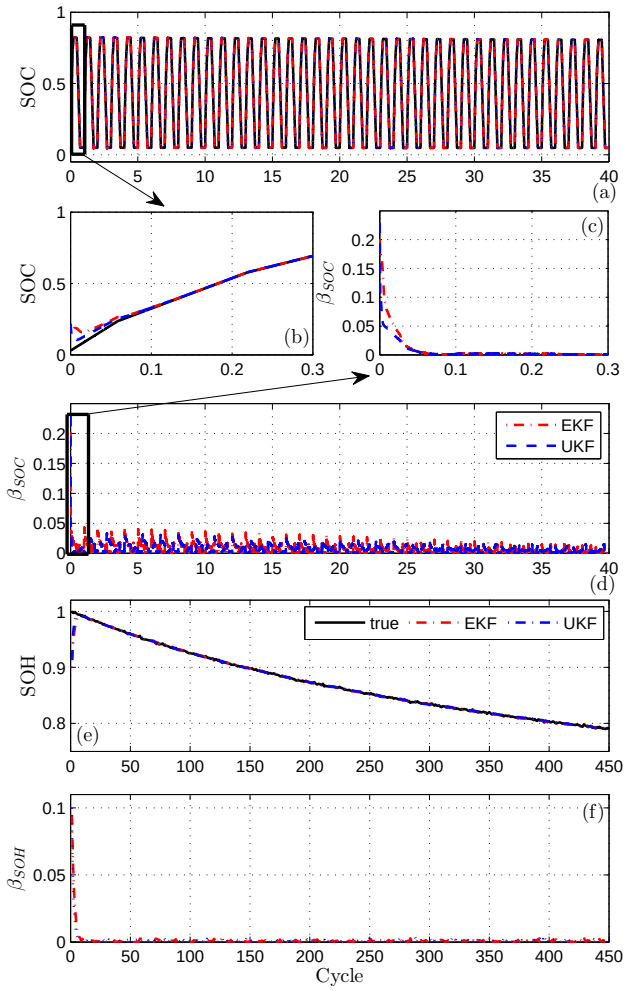

Figure 8: Estimation results of the SOC and SOH in multi-time-scales. (a) The true SOC (black solid line) and its estimated values from the EKF (red dot-dashed line) and UKF (blue dotted line). (d). The relative absolute error in SOC estimation. (b) and (c) are separately the zoom-in figures of (a) and (d) in their first cycle. (e) and (f) are the SOH profiles and respective estimation errors.

5. Conclusion

In this paper, a multi-time-scale estimation was proposed for state estimation in a class of singularly perturbed systems. Assumptions imposed on the internal models and the estimation error dynamic systems were explicitly stated. It has been analytically proved that under these assumptions, an appropriately designed estimator is able to compensate the uncertainties including modelling errors brought about by time-scale separation.

This proposed algorithm was applied to a lithium-ion battery for estimation of the SOC and SOH. Starting from physics-based high-fidelity battery models, reduction techniques are systematically applied to develop appropriate models that capture the key system characteristics but are computationally efficient. Based on these obtained models, the capability of this estimation framework has been demonstrated using both EKF and UKF. Simulation results have shown that the designed observers are effective in the presence of initial error, model mismatch, and measurement noise. Furthermore, the established methodology for state estimation of singularly perturbed systems is very general so that it can be applied to other battery chemistries where proper models exist.

An important next step is to experimentally validate the proposed observer over statistically significant trials and consider how to integrate it into battery monitoring packs. Furthermore, it may be able to develop model-based battery management system to pursue optimal charging strategies.

Acknowledgment

This work was partially supported by the National Information Communication Technology, Australia (NICTA), and Australian Research Council through grant FT100100538. The authors would also like to thank Prof. Xiaosong Hu from Chongqing University and Dr. Satadru Dey from University of California, Berkeley for their valuable assistance and support.

[1] M. J. Brear, P. Dennis, C. Manzie, R. Sharma, SAE Journal of Passenger Cars 6 (1) (2013) 61–77.
[2] N. P. Balsara, and J. Newman, J. Chemical Education 90.4 (2013) 446–452.
[3] C. Zou, A. G. Kallapur, C. Manzie, D. Nešić, IEEE Conference on Decision and Control, (2015) 1328–1333.
[4] N. A. Chaturvedi, R. Klein, J. Christensen, J. Ahmed, A. Kojic, IEEE Control System Magazine 30 (3) (2010) 49–68.
[5] C. Zou, C. Manzie, D. Nešić, IEEE Trans. Control Systems Technology 24 (5) (2016) 1594–1609.
[6] C. Zou, C. Manzie, D. Nesic, Asian Control Conference, (2015) 2355–2360.
[7] N. Kazantzis, N. Huynh, R. A. Wright, Computers & Chemical Engineering 29 (4) (2005) 797–806.
[8] H. He, R. Xiong, X. Zhang, F. Sun, J. Fan, Vehicular Technology, IEEE Transactions on 60 (4) (2011) 1461–1469.
[9] F. Sun, X. Hu, Y. Zou, S. Li, Energy 36 (5) (2011) 3531–3540.
[10] A. Singh, A. Izadian, S. Anwar, J. Power Sources 268 (2014) 459–468.
[11] X. Chen, W. Shen, Z. Cao, A. Kapoor, J. Power Sources 246 (2014) 667–678.
[12] B. Saha, K. Goebel, S. Poll, J. Christophersen, IEEE Trans. Instrumentation and Measurement 58 (2) (2009) 291–296.
[13] Y. Zou, X. Hu, H. Ma, S. E. Li, J. Power Sources 273 (1) (2015) 793–803.
[14] L. Ji, G. Li, and H. K. Fathy, J. Dynamic Sys., Meas., and Control 138, no. 2 (2016): 021009.
[15] M. Muratori, M. Canova, Y. Guezennec, G. Rizzoni, IFAC Symposium Advances in Automotive Control (2010) 11–14.
[16] J. C. Forman, S. Bashash, J. L. Stein, H. K. Fathy, J. Electrochemical Society 158 (2) (2011) A93– A101.
[17] S. Dey, B. Ayalew, American Control Conference (2014) 248–253.
[18] D. Di Domenico, A. Stefanopoulou, G. Fiengo, J. Dynamic Sys., Meas., and Control 132 (6) (2010) 061302.
[19] S. J. Moura, N. A. Chaturvedi, M. Krstic, J. Dynamic Sys., Meas., and Control 136 (1) (2014) 011015.
[20] S. Javid, IEEE Conference on Decision and Control including the Symposium on Adaptive Processes 18 (1979) 853–854.
[21] M. S. Mahmoud, H. K. Khalil, Automatica 38 (2) (2002) 361–369.
[22] A. R. Teel, L. Moreau, and D. Nesic, IEEE Trans. Autom. Control, 48 (9) (2003) 1526–1544.
[23] L. Cuevas, D. Nesic, and C. Manzie, IEEE Conference on Decision and Control, (2015) *under review*.
[24] H. K. Khalil, Nonlinear Control: Global edition, Vol. 1, Pearson Education Limited, (2014).
[25] P. V. Kokotovic, H. K. Khalil,, and J. O'reilly. Siam 25 (1999).
[26] C. Zou, C. Manzie, and S. Anwar, IFAC World Congress, (2014) 3912–3917.

[27] V. R. Subramanian, V. D. Diwakar, D. Tapriyal, J. Electrochemical Society 152 (10) (2005) A2002–A2008.
[28] W. Luo, C. Lyu, L. Wang, L. Zhang, Microelectronics Reliability 53 (6) (2013) 797–804.
[29] P. Ramadass, B. Haran, P. M. Gomadam, R. White, B. N. Popov, J. Electrochemical Society 151 (2) (2004) A196–A203.
[30] S. Buller, M. Thele, R.W.A.A. De Doncker, and E. Karden, IEEE Trans. Ind. Appl 41 (3) (2005) 742–747.
[31] S. J. Julier, J. K. Uhlmann, International Society for Optics and Photonics, (1997) 182–193.